Expanded View Figures

Figure EV1. Hel2 and Ubc4 were involved in NGD but not NSD and NMD.

A Schematic drawing of reporter mRNAs containing various arrest-inducing sequences. The box indicates *GFP* and *HIS3* open reading frames (ORFs), and the black line indicates the untranslated region (UTR). Ribosome stalling takes place during translation of the indicated arrest sequences (shown in red) and induces an endonucleolytic cleavage to produce two fragments, the 5′ NGD intermediate (5′ NGD-IM) and 3′ NGD intermediate (3′ NGD-IM).

B Northern blot analysis showing that Hel2 is required for endonucleolytic cleavages by $R(CGN)_{12}$ arrest-inducing sequences. The *GFP-R(CGN)$_{12}$-HIS3* mRNA (FL) and the 5′ NGD-IM were detected in the indicated strains using a DIG-labelled *GFP* probe. *SCR1* coding for RNA in the signal recognition particle (SRP) was used as a loading control.

C Northern blot analysis showing that Ubc4 but not Ubc5 is required for endonucleolytic cleavages by $R(CGN)_{12}$ arrest-inducing sequences. The *GFP-R(CGN)$_{12}$-HIS3* mRNA (FL) and the 5′ NGD-IM were detected in the indicated strains with the DIG-labelled *GFP* probe.

D Northern blotting showing that Hel2 and Ubc4 are required for endonucleolytic cleavages by $R(CGN)_{12}$ arrest-inducing sequences. The *GFP-R(CGN)$_{12}$-HIS3* mRNA (FL) and the 3′ NGD-IM were detected in the indicated strains with the DIG-labelled *HIS3* probe.

E Northern blotting showing that Hel2 reduces the half-life of reporter mRNA containing *R(CGN)$_{12}$* or *K(AAA)$_{12}$* arrest sequences. The stability of *GFP-K(AAA)$_{12}$-FLAG-HIS3* and *GFP-R(CGN)$_{12}$-FLAG-HIS3* mRNAs was determined. The *GFP-K(AAA)$_{12}$-FLAG-HIS3* mRNA was stable in *hel2* mutant cells than that in wild-type cells ($t_{1/2}$ = 11.2 min for *hel2*Δ versus $t_{1/2}$ = 4.3 min for wild type). The *GFP-R(CGN)$_{12}$-FLAG-HIS3* mRNA was also stable in *hel2* mutant cells than that in wild-type cells ($t_{1/2}$ = 7.6 min for *hel2* versus $t_{1/2}$ = 4.9 min for wild type). In contrast, the stability of *GFP-K(AAA)$_{12}$-FLAG-HIS3* mRNA was essentially the same in *hel2* mutant cells ($t_{1/2}$ = 6.0 min) and in wild-type cells ($t_{1/2}$ = 5.8 min). This stabilization of the reporter mRNAs that are substrate for NGD in *hel2* mutant cells strongly supports the crucial role of Hel2 in NGD. On the other hand, mRNA stability did not change in *slh1*Δ and *uS10-K6/8R* mutant cells.

F Hel2 is dispensable for NSD and NMD. The *GFP-Rz* mRNA is a truncated poly(A) tail-less non-stop mRNA that is produced by self-cleavage of hammerhead ribozyme (Rz) and efficiently degraded in the NSD pathway (Tsuboi *et al*, 2012). The *FLAG-HIS3-NS* mRNA is a poly(A) tail containing nonstop mRNA and subjected to NSD (van Hoof *et al*, 2002). The *FLAG-his3-100* mRNA contains premature termination codon and degraded by NMD quality control (Kuroha *et al*, 2009). The relative levels of reporter mRNAs in the indicated mutant cells were determined using a DIG-labeled *GFP* (*GFP-Rz*) or 5′ DIG-labeled-LNA-FLAG (*FLAG-HIS3-NS* or *FLAG-his3-100*) probes. The relative levels of each mRNA were normalized to the mRNA level in time 0, which was assigned a value of 100, and *SCR* RNA levels were used as a loading control for the RNA samples.

G Western blot analysis to check the expression levels of HA-tagged Hel2 deletion mutant proteins as schematically displayed in Fig 1B using an anti-HA antibody.

© 2018 The Authors

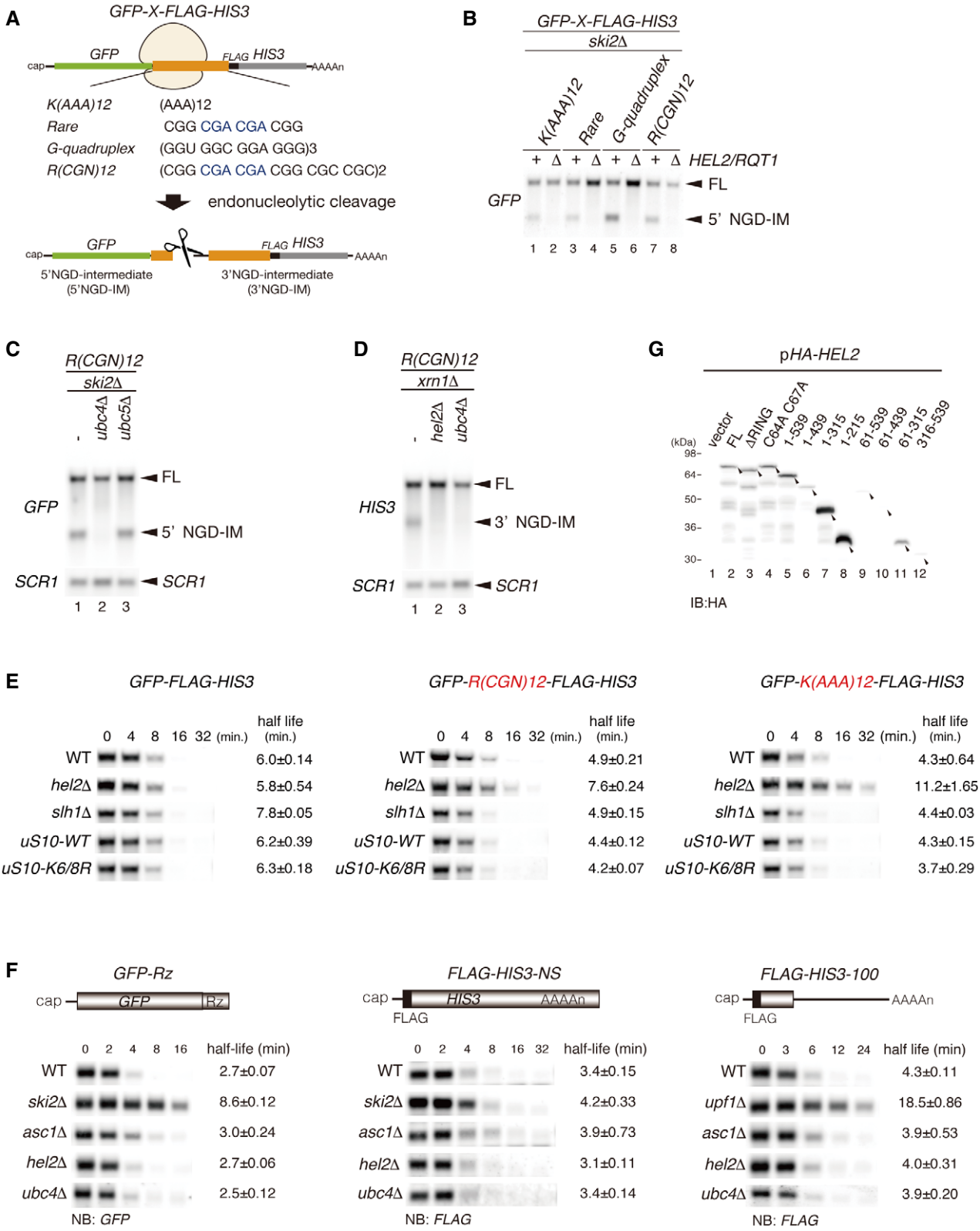
A
GFP-X-FLAG-HIS3
cap
GFP
FLAG HIS3
AAAAn
K(AAA)12 (AAA)12
Rare CGG CGA CGA CGG
G-quadruplex (GGU GGC GGA GGG)3
R(CGN)12 (CGG CGA CGA CGG CGC CGC)2
endonucleolytic cleavage
5'NGD-intermediate (5'NGD-IM)
3'NGD-intermediate (3'NGD-IM)
B
GFP-X-FLAG-HIS3
ski2Δ
K(AAA)12
Rare
G-quadruplex
R(CGN)12
HEL2/RQT1
GFP
FL
5' NGD-IM
C
R(CGN)12
ski2Δ
ubc4Δ
ubc5Δ
GFP
SCR1
D
R(CGN)12
xrn1Δ
hel2Δ
ubc4Δ
HIS3
3' NGD-IM
G
pHA-HEL2
vector
FL
ΔRING
C64A C67A
1-539
1-439
1-315
1-215
61-539
61-439
61-315
316-539
(kDa)
98-
64-
50-
36-
30-
IB:HA
E
GFP-FLAG-HIS3
GFP-R(CGN)12-FLAG-HIS3
GFP-K(AAA)12-FLAG-HIS3
half life (min.)
WT 6.0±0.14 4.9±0.21 4.3±0.64
hel2Δ 5.8±0.54 7.6±0.24 11.2±1.65
slh1Δ 7.8±0.05 4.9±0.15 4.4±0.03
uS10-WT 6.2±0.39 4.4±0.12 4.3±0.15
uS10-K6/8R 6.3±0.18 4.2±0.07 3.7±0.29
F
GFP-Rz
FLAG-HIS3-NS
FLAG-HIS3-100
half-life (min)
WT 2.7±0.07 3.4±0.15 4.3±0.11
ski2Δ 8.6±0.12 4.2±0.33
upf1Δ 18.5±0.86
asc1Δ 3.0±0.24 3.9±0.73 3.9±0.53
hel2Δ 2.7±0.06 3.1±0.11 4.0±0.31
ubc4Δ 2.5±0.12 3.4±0.14 3.9±0.20
NB: GFP
NB: FLAG
NB: FLAG

Figure EV1.

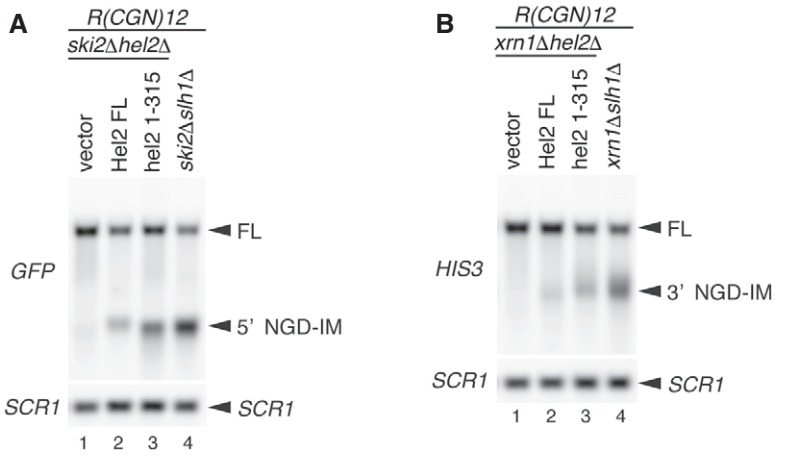

Figure EV2. Alteration of mRNA cleavage sites in Hel2(1–315) expressing cells.

A, B Northern blot showing that the length of 5′ NGD intermediate was altered in Hel2(1–315) expressing cells and *slh1Δ* cells. The full-length *GFP-R(CGN)$_{12}$-FLAG-HIS3* mRNA and 5′ NGD intermediates (5′ NGD-IM) or 3′ NGD intermediates (3′ NGD-IM) were detected in the indicated mutant cells with expression of Hel2 wild-type or 1–315 mutant from plasmid by Northern blotting with DIG-labelled probes. 5′ NGD intermediates were detected by DIG-labelled *GFP* probe in (A), and 3′ NGD intermediates were detected by the DIG-labelled *HIS3* probe in (B). *SCR1* is used as loading control. FL; full length. Note an upstream shift of NGD cleavage sites in lanes A3-4 and B3-4.

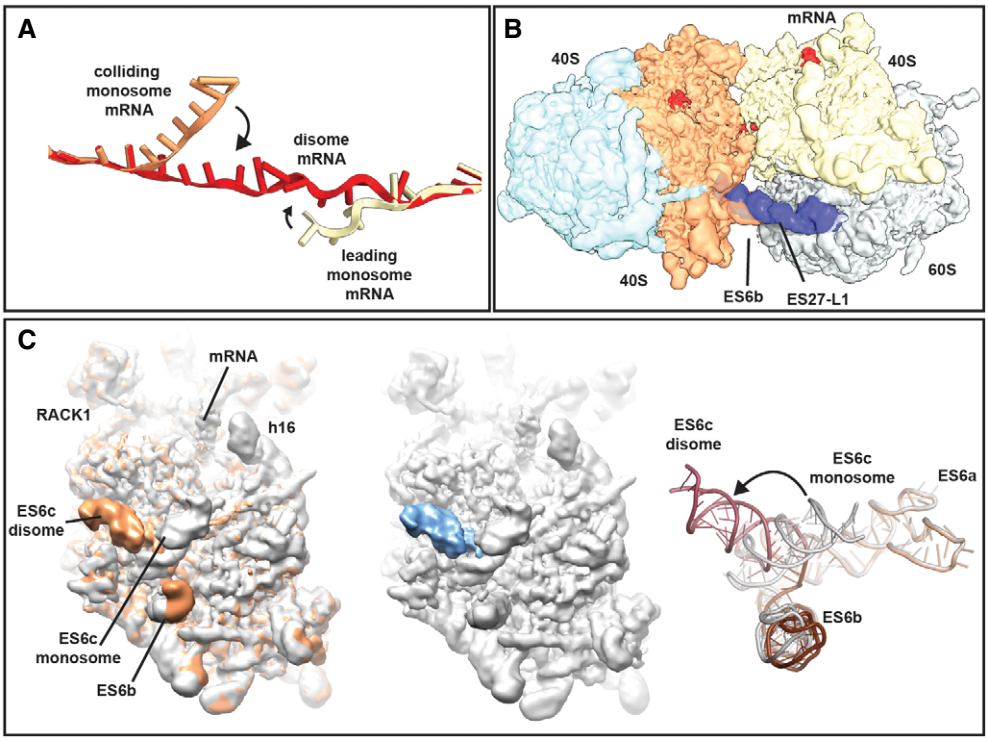

Figure EV3. Conformational rearrangements in the disome.

A mRNA was modelled into the refined maps of the hybrid A/P-P/E tRNA containing monosome and the P/P tRNA containing monosome with ES27 in the L1 conformation (see Appendix Figs S4 and S6). These ribosomes are not involved in disome formation and show density for mRNA in covering approximately 30 nucleotides in the canonical path. In the disome, the mRNA deviates from the canonical path at the exit site of 5′ mRNA and at the entry site of the 3′-mRNA in the colliding ribosome. In the disome, the corresponding nucleotides are stretching out to connect leading and colliding ribosome.

B Superposition of the disome map shown as in Fig 4A with the isolated ES27 density from the refine monosome sub-class representing the P/P tRNA containing ribosome with ES27 in the L1 position (blue). Note that ES27 would clash with the 60S-40S disome bridge involving ES6b.

C Left panel: superposition of the refined colliding ribosome from the disome (yellow orange) with the hybrid A/P-P/E tRNA containing monosome (grey; see Appendix Figs S4 and S6). The view focuses on ES6. Middle panel: superposition of hybrid A/P-P/E tRNA containing monosome with the difference map. Note that the only significant difference is in ES6c. Right panel: superposition of molecular models for ES6 in a disome (dark red/brown) and in a monosome (grey).

 © 2018 The Authors

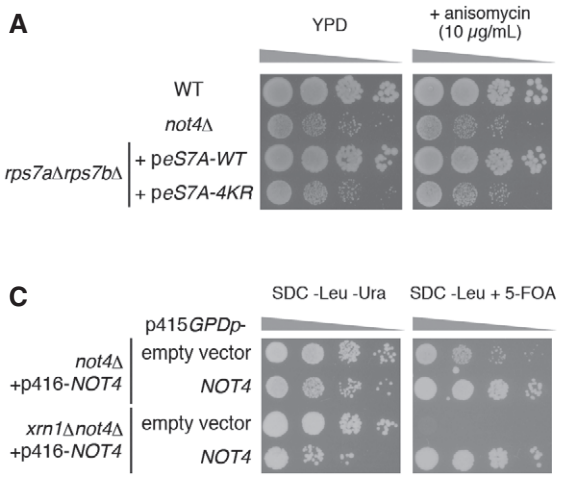

Figure EV4. Genetic interactions between *NOT4* and quality control factors.

A Spot assay showing that severe growth defect of *not4*Δ and *eS7A-4KR* mutant cells irrespective of the presence of anisomycin. Indicated yeast cells were cultured with liquid YPD media, and 10-fold serial dilutions of the cells were grown on YPD with or without 10 μg/ml anisomycin.

B Spot assay showing that *not4*Δ*hel2*Δ and *not4*Δ*slh1*Δ exhibited synthetic growth defect. Indicated yeast cells were cultured with liquid YPD media, and then, 10-fold serial dilutions of the cells were grown on YPD.

C Synthetic lethality of *xrn1*Δ*not4*Δ cells. Spot assay of *not4*Δ and *xrn1*Δ*not4*Δ yeast cells harbouring p416*GPDp-FLAG-NOT4* transformed with p415*GPD* empty vector or p415*GPDp-FLAG-NOT4*. Transformed cells on the SDC-Leu medium were cultured with liquid SDC-Leu media for 1 day, and 10-fold serial dilutions of the cells were grown on SDC-Leu-Ura plate or SDC-Leu plate with 0.5 g/l 5-fluoroorotic acid (5-FOA).

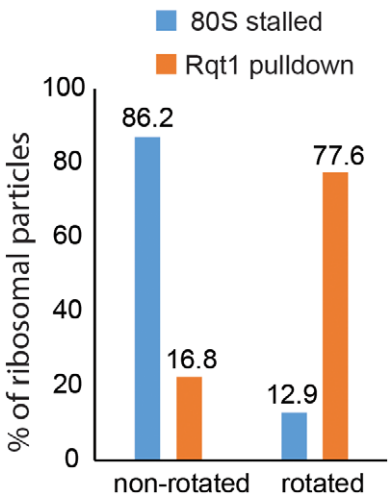

Figure EV5. Comparison of ribosomal states in Hel2 pulldown and CGA-CCG-stalled monosomes (80S).

Hel2 preferentially interacted with rotated A/P-P/E ribosomes (77.6%). Ribosomes in this state are almost not present in the case of leading stalled 80S where 86.2% ribosomal particles are in the P/P E/E non-rotated state. Therefore, Hel2 seems to preferentially interact with colliding stalled ribosomes.

© 2018 The Authors